Available online at www.sciencedirect.com
SCIENCE DIRECT®
European Journal of Mechanics B/Fluids 23 (2004) 607–616

The flow induced by Prandtl's self-similar vortex sheet spirals at infinite distance from the spiral kernel

G.A.M. van Kuik

Delft University, Wind Energy Research Institute, Stevinweg 1, 2628 CN Delft, The Netherlands

Received 7 April 2003; received in revised form 16 December 2003; accepted 19 January 2004
Available online 9 April 2004

Abstract

Prandtl's (Über die Entstehung von Wirbeln in der idealen Flüssigkeit, mit Anwendung auf die Tragflügeltheorie und andere Aufgaben, Springer, Berlin, 1922) self-similar vortex sheets are characterized by unsteady flow around an exponential spiral with an invariant shape. Discussions in the literature show that Prandtl's solutions are not well-posed for the behavior of the vortex strength at infinity. This discussion is continued here by analyzing the flow at infinity. To introduce a length scale, firstly the flow around an exponential spiral with a finite length is derived. In the limit for infinite spiral length, Prandtl's equations are recovered, but now include the flow properties at infinity. The flow requires a description in a multi-branched Riemann surface. In a 2-D representation the flow is discontinuous across the branch line. In the limit for the infinite spiral, this discontinuity moves to infinity. Therefore, the Prandtl spirals cannot be described as a 2-D flow.

Keywords: Spiral; Vortex sheets; Prandtl; Similarity solution

1. Introduction

1.1. Similarity solutions for rolled-up 2-D vortex sheets

The roll-up process of two-dimensional, semi-infinite vortex sheets has been modelled by many researchers using similarity solutions of the form: $r \sim t^m f(\theta)$, where r and θ are the polar coordinates, t the time and m and $f(\theta)$ the unknowns. Kaden [1] derived a solution for a sheet behind an elliptically loaded wing. The vortex sheet rolls up in a spiral, of which the turns become more and more circular near the kernel. The time constant for this solution is $m = 2/3$, giving $r \sim (t/\theta)^{2/3}$. The Kaden type of spirals has been reproduced for vortex sheets created by non-elliptic wing loadings, by numerical calculations as well as by experiments. Saffman [2] identifies two families of similarity solutions for two ranges of m. For $m > 1/2$ the solutions are spirals like the Kaden spiral, with almost circular turns near the kernel. For the range $m < 1/2$ equi-angular spirals $r \sim t^m \, \mathrm{e}^{\theta}$ are found by Prandtl [3] and Alexander [4]. These spirals have the same shape for all θ, apart from the scale. The physical interpretation of Prandtl's class of spirals is not clear. The evolution of vortex sheets of the Kaden as well as Prandtl type is discussed in detail by Küchemann and Weber [5], Mangler and Weber [6] and Saffman [2]. More recently, Prandtl's self-similar vortex sheets have been analyzed by Kambe [7] and Kaneda [8]. Kambe has shown that, although Prandtl's exponential spiral vortex sheets satisfy local conditions (expressed by the Birkhoff–Rott equation) the similarity solutions are not well-posed for the behavior of vortex strength at infinity. This reason for this is that the circulation per unit length diverges at infinity. Kambe's conclusions are confirmed by Kaneda who generalized Alexander's solutions to a family of analytical solutions of double-branched spiral vortex sheets in which the spirals themself are allowed to move.

E-mail address: g.vankuik@citg.tudelft.nl (G.A.M. van Kuik).

0997-7546/$ – see front matter
doi:10.1016/j.euromechflu.2004.01.002

1.2. Prandtl's self-similar spirals

Prandtl [3] published the potential flow solution for a class of two-dimensional, semi-infinite, rolled-up vortex sheets, of which the shape is invariant in time. Prandtl distinguishes two types of flows. The first type concerns flows in which the spiral keeps its shape but moves as a whole ('ähnlich veränderlich' according to Prandtl). The time dependent complex potential χ is:

$$\chi(t,z) = ct^{2m-1}\left(\frac{z}{t^m}\right)^{\alpha+\mathrm{i}\beta}, \tag{1}$$

where $\chi(t,z) = \Phi(t,z) + \mathrm{i}\Psi(t,z)$, Φ the potential function, Ψ the stream function, $z = r\,\mathrm{e}^{\mathrm{i}\theta}$ the complex coordinate and t the time. The constants c, m, α and β are to be determined. The second type concerns unsteady flows in which the spiral has a fixed position ('kongruent veränderlich'), defined by:

$$\chi(t,z) = ct^{2m-1}z^{\alpha+\mathrm{i}\beta}. \tag{2}$$

For $m = 0$ both types become identical. Expressed in polar coordinates (r,θ) the shape of the sheet is given by Prandtl:[1]

$$r_{\text{spiral}} = \mathrm{e}^{-\frac{\alpha}{\beta}\theta_{\text{spiral}}}, \tag{3}$$

which is shown in Fig. 1. The spirals are semi-infinite by which no length scale is involved.

The constants α and β are determined by Prandtl and others by applying the kinematic and dynamic boundary condition (no cross flow, no pressure jump across the sheet, conservation of vorticity). This is repeated in Appendix A. The kinematic boundary condition is easily derived for all m, resulting in the requirement (A.5) for α: $\sin(2\pi\alpha) = 0$. The dynamic boundary condition can be evaluated analytically only for $m = 0$, leading to the requirement (A.11): $\alpha^2 + \beta^2 - 2\alpha = 0$. With known α and β the constant c is also determined by the dynamic condition. Alexander [4] extended Prandtl's solution for $m = 0$, $\alpha = \frac{1}{2}$, $\beta = -\frac{1}{2}\sqrt{3}$ to other values of the ratio α/β and to multi-branched spirals. These spirals and the associated flow remain unchanged by a rotation of the coordinates through an angle of $2\pi/N$, where N is the number of branches. Eq. (1) still holds for this case, with N entering the solutions for α and β. Table 1 presents the parameters of all possible analytic solutions of (1) and (2) for single-branched spirals with a fixed position. The inclination angle δ is defined as the angle between the normal and the radius vector from the centre, see Fig. 1.

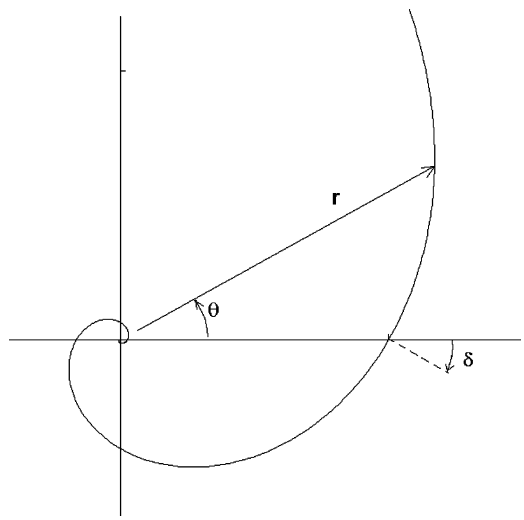

Fig. 1. The complex z-plane, with the semi-infinite exponential spiral $r = \mathrm{e}^{\theta/\sqrt{3}}$ (Eq. (3), with $\alpha = \frac{1}{2}$, $\beta = -\frac{1}{2}\sqrt{3}$). The inclination angle $\delta = 30°$.

[1] The orientation of Prandtl's spiral is opposite to that shown in Fig. 1. Therefore he found a positive value for β. The values in Table 1 and the text are according to the orientation in this paper: an increasing radius for increasing polar angle.

Table 1
The constants defining the solutions of (1) and (2) for $m = 0$

	α	β	δ	c
Prandtl [3]	$\frac{1}{2}$	$-\frac{1}{2}\sqrt{3}$	30°	$2\frac{1+e^{\pi\sqrt{3}}}{1-e^{2\pi\sqrt{3}}}$
Alexander [4]	1	-1	45°	$\frac{1-e^{2\pi}}{1-e^{4\pi}}$
Alexander [4]	$1\frac{1}{2}$	$-\frac{1}{2}\sqrt{3}$	60°	$\frac{2}{3}\frac{1+e^{\pi\sqrt{3}}}{1-e^{2\pi\sqrt{3}}}$

1.3. Interpretation problems of Prandtl's spirals

For the spirals with a fixed position, the time derivative of the potential (2) can be written as $\partial\chi/\partial t = (2m-1)\chi/t$. Consequently, all kinematic quantities, like the vortex sheet strength γ and the circulation Γ, behave similarly, so:

$$\frac{\partial \Gamma_s}{\partial t} = (2m-1)\frac{\Gamma_s}{t} \quad \text{for spirals with a fixed position} \tag{4}$$

for any spiral position s. Consequently, the circulation increases to infinite values. Prandtl as well as Smith [9] explain this by stating that the spiraling vortex sheet emanates continuously from the trailing edge of an aerofoil. This source of vorticity is not modelled in Prandtl's analysis. Consequently, the spirals have the special property that the total circulation is time-dependent, while the conservation of vorticity is satisfied at all positions along the spiral.

A topic which is not discussed so far, is the non-periodicity of the flow in the polar angle θ. Substitution of $\theta^* = \theta + 2\pi$ in (1) or (2) gives $\chi(t, z^*) = e^{2\pi(i\alpha-\beta)}\chi(t, z)$, yielding the same flow field but multiplied by the complex constant $e^{2\pi(i\alpha-\beta)}$. This implies a rotation about an angle $2\pi\alpha$ as well as a scaling with a factor $e^{-2\pi\beta}$ so the potential is single-valued for only one full turn of θ. The potential becomes single-valued for all turns (branches) of θ when these branches are coupled by a Riemann surface: a two-dimensional but multi-branched surface like an Archimedes- or corkscrew for which each 2π increase of θ results in a position at a new branch of the spiraling surface. Fig. 5, which will be discussed in Section 2.2, is an example with two branches shown. A plane 2-D representation of only one 2π-turn of θ implies the definition of a branch line, which marks the transition to the adjacent branches. Multi-valued flows like $\chi(z) = \ln z$ show a discontinuity in flow properties across the branch line. The interpretation problem of the Prandtl spirals is that the flow is non-periodic and at the same time satisfies all boundary conditions.

The analysis in this paper adresses the conditions at infinity and the non-periodicity, and is entirely kinematic. Since the dynamic boundary condition is not used and the kinematic properties of both types of spirals are similar, a unified complex potential w is defined for both flow types. With substitution of $\tilde{z} = z/t^m$ in (1), the expressions (1) and (2) become equal:

$$\chi(t, \tilde{z}) = t^{2m-1} w(\tilde{z}), \tag{5}$$

$$w(\tilde{z}) = c\tilde{z}^{\alpha+i\beta}, \tag{6}$$

$$\tilde{z} = z \quad \text{for the fixed spiral,} \tag{7}$$

$$\tilde{z} = \frac{z}{t^m} \quad \text{for the moving spiral.} \tag{8}$$

All kinematic quantities are determined by (6)–(8), expressed in the coordinate $\tilde{z}$. In the remainder of this paper the complex potential (6) is used as basis for the analysis. All results need to be converted through (5), (7), (8) to be applicable for both spiral types. *For simplicity, the symbol ˜ is omitted in the remainder of this paper.*

To define flow properties at infinity, the flow induced by an exponential spiral with finite length is determined. Then the limit for infinite spiral length is taken to recover Prandtl's formulation. In this way a length scale is introduced, which is absent in Prandtl's analysis. This length scale enables the derivation of the flow conditions at infinity.

2. The potential flow solution for exponential spirals of finite length

2.1. The similarity between the flat plate flow and the spiral flow

Alexander [4] mentions the similarity between the flow around a semi-infinite flat plate and the flow around the semi-infinite exponential spiral. We define the flat plate flow in the ζ-plane, Fig. 2, and the spiral flow in the z-plane, Fig. 3. Indeed the transformation:

$$z^{\alpha+i\beta} = \zeta^2 \tag{9}$$

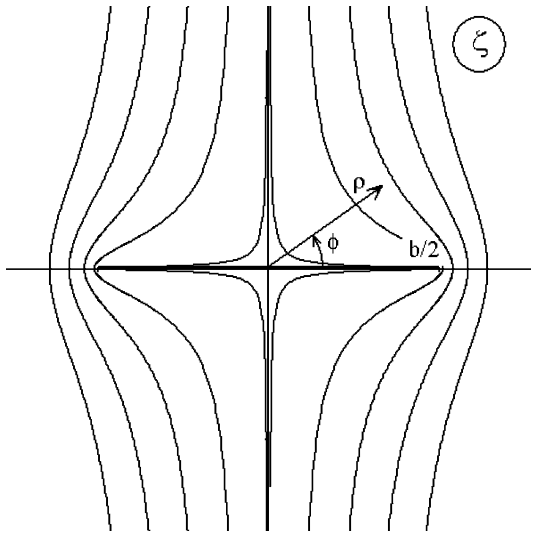

Fig. 2. The complex ζ-plane: the flow around a flat plate. The streamlines shown correspond to the following values of the streamfunction Ψ, which is non-dimensionalized with the plate half-width and the undisturbed velocity: $\Psi = 0.01, 0.2, 0.4, 0.6, 0.8$.

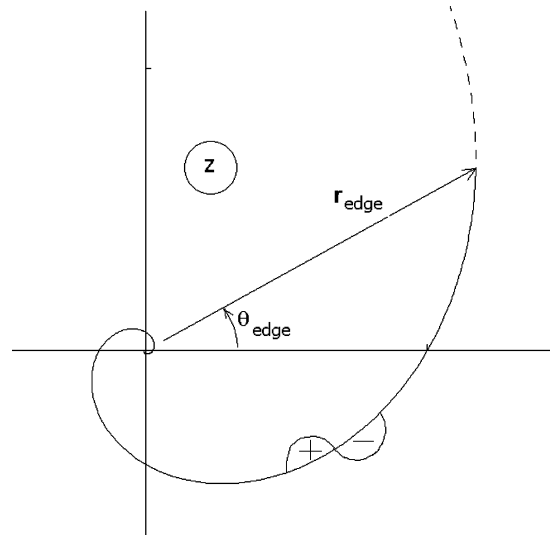

Fig. 3. The spiral with finite length in the z-plane, with $\alpha = \frac{1}{2}$, $\beta = -\frac{1}{2}\sqrt{3}$. The dashed line is the branch line in the Riemann surface.

maps the flat plate flow into a spiral flow, as will be shown. Assume a finite flat plate with length b and undisturbed velocity U_0 perpendicular to the blade. Then the complex potential is:

$$w(\zeta) = \mathrm{i}U_0\sqrt{\zeta^2 - \left(\frac{b}{2}\right)^2}. \tag{10}$$

Substitution of the transformation (9) yields the flow in the z-plane defined by the complex potential:

$$w(z) = \mathrm{i}U_0\sqrt{z^{\alpha+\mathrm{i}\beta} - \left(\frac{b}{2}\right)^2}. \tag{11}$$

For small $|z|$ or large b the complex potential (11) can be written as a series expansion with respect to b^{-1}:

$$w(z) = -U_0\frac{b}{2}\left[1 - \frac{1}{2}\frac{z^{\alpha+\mathrm{i}\beta}}{(b/2)^2} + \frac{1}{8}\frac{z^{2(\alpha+\mathrm{i}\beta)}}{(b/2)^4} - \cdots\right] = U_0\left[-\frac{b}{2} + \frac{1}{b}z^{\alpha+\mathrm{i}\beta} - \frac{1}{b^3}z^{2(\alpha+\mathrm{i}\beta)}\cdots\right]. \tag{12}$$

Apart from the constant term which can be omitted, the first term in (12) indeed equals the complex potential (6). This semi-infinite-spiral-flow appears to be the first relevant term in the series expansion of the finite-spiral-flow with respect to b^{-1}. By comparison with (12) the constant c in (6) is expressed in terms of the parameters that define the length and time scale:

$$c = \frac{U_0}{b}. \tag{13}$$

2.2. The finite spiral flow

First the shape of the finite spiral is derived. With $\zeta = \rho\,\mathrm{e}^{\mathrm{i}\varphi}$ and $z = r\,\mathrm{e}^{\mathrm{i}\theta}$, the mapping (9) becomes:

$$r^{\alpha}\,\mathrm{e}^{-\beta\theta}\,\mathrm{e}^{\mathrm{i}(\alpha\theta)+\beta\ln r} = \rho^2\,\mathrm{e}^{\mathrm{i}2\varphi}, \tag{14}$$

or:

$$\begin{aligned}(\alpha^2+\beta^2)\theta &= 2(-\beta\ln\rho + \alpha\varphi),\\ (\alpha^2+\beta^2)\ln r &= 2(+\alpha\ln\rho + \beta\varphi).\end{aligned} \tag{15}$$

The horizontal axis in the ζ-plane, defined by $\varphi = n\pi$, n integer, is transformed to the spiral:

$$r_{\text{spiral}} = \mathrm{e}^{-(\alpha/\beta)(\theta_{\text{spiral}} - 2n\pi/\alpha)}. \tag{16}$$

The shape is characterized by the inclination angle δ being the angle between the normal and the radius vector from the centre, see Fig. 1:

$$\delta = \arctan\left(-\frac{\alpha}{\beta}\right). \tag{17}$$

The position of the edge is given by substitution of $\rho = b/2$, $\varphi = n\pi$ in (15):

$$r_{\text{edge}} = \left(\frac{b}{2}\right)^{2\alpha/(\alpha^2+\beta^2)} \mathrm{e}^{2n\pi\beta/(\alpha^2+\beta^2)}, \tag{18}$$

$$\theta_{\text{edge}} = \ln\left(\frac{b}{2}\right)^{-2\beta/(\alpha^2+\beta^2)} + \frac{2n\pi\alpha}{\alpha^2+\beta^2}. \tag{19}$$

For $n = 0$, this simplifies to

$$z_{\text{edge},\ n=0} = \left(\frac{b}{2}\right)^{2(\alpha-\mathrm{i}\beta)/(\alpha^2+\beta^2)}. \tag{20}$$

The edge of the spiral carries a suction force, equivalent to the suction force at the edge of the flat plate, see Appendix B.

The length ℓ of the spiral is, for $n = 0$:

$$\ell_{n=0} = \int_{-\infty}^{\theta_{\text{edge}}} \sqrt{r_{\text{spiral}}^2 + \left(\frac{\mathrm{d}r_{\text{spiral}}}{\mathrm{d}\theta_{\text{spiral}}}\right)^2}\,\mathrm{d}\theta_{\text{spiral}} = \sqrt{1+\left(\frac{\alpha}{\beta}\right)^2}\, r_{\text{edge}} = \sqrt{1+\left(\frac{\alpha}{\beta}\right)^2}\left(\frac{b}{2}\right)^{2\alpha/(\alpha^2+\beta^2)}. \tag{21}$$

Eq. (16) shows that (9) is multi-valued: $\varphi = 0$ yields the spiral $r_{\text{spiral}} = \mathrm{e}^{-(\alpha/\beta)\theta_{\text{spiral}}}$ whereas $\varphi = 2\pi$ yields $r_{\text{spiral}} = \mathrm{e}^{-(\alpha/\beta)(\theta_{\text{spiral}}-4\pi/\alpha)}$. This can be summarized as:

$$\left[\varphi_0 \leqslant \varphi \leqslant (\varphi_0 + 2\pi)\right]_\zeta \text{ corresponds to } \left[\theta_0 \leqslant \theta \leqslant \left(\theta_0 + \frac{4\pi}{\alpha}\right)\right]_z \tag{22}$$

with

$$\left[r_0 \leqslant r_{\text{spiral}} \leqslant r_0\,\mathrm{e}^{-4\pi/\beta}\right]_z. \tag{23}$$

The expression for the conjugate velocity is:

$$\frac{\partial w(z)}{\partial z} = U_0 \frac{\mathrm{i}(\alpha+\mathrm{i}\beta) z^{\alpha+\mathrm{i}\beta-1}}{2\sqrt{z^{\alpha+\mathrm{i}\beta} - (b/2)^2}}. \tag{24}$$

With (17) rewritten as:

$$\mathrm{i}(\alpha+\mathrm{i}\beta) = \sqrt{\alpha^2+\beta^2}\,\mathrm{e}^{\mathrm{i}\delta} \tag{25}$$

and substitution of (20), (24) becomes:

$$\frac{\partial w(z)}{\partial z} = U_0 \frac{b}{4}\sqrt{\alpha^2+\beta^2}\,\frac{(z/z_{\text{edge}})^{\alpha+\mathrm{i}\beta}}{\sqrt{1-(z/z_{\text{edge}})^{\alpha+\mathrm{i}\beta}}}\,\frac{\mathrm{e}^{\mathrm{i}(\delta-\pi/2)}}{z}. \tag{26}$$

This describes the velocity at each position z. Since the mapping (9) is multi-valued, this also holds for (26). As an example, the flow pattern of the spiral with an inclination angle of 30° ($\alpha = \frac{1}{2}$, $\beta = -\frac{1}{2}\sqrt{3}$) is shown in Fig. 4. This flow pattern is derived using the analytical solution for the flat plate flow streamlines given by Lamb [10], and the transformation (9). We assume $b/2 = 1$, so the edge position is given by (20): $r_{\text{edge}} = 1$, $\theta_{\text{edge}} = 0$. Expression (22) shows that each period $\theta_0 \leqslant \theta \leqslant \theta_0 + 2\pi$ in the z-plane is the transformation of one quadrant of the ζ-plane. Fig. 4 shows the flow, being the mapping of the flow in the quadrants in the ζ-plane defined by $-\pi/2 \leqslant \varphi \leqslant 0$ (right part) and $0 \leqslant \varphi \leqslant \pi/2$ (left part). The mapping of the other quadrants in the ζ-plane gives identical results but reduced by a scale factor $\mathrm{e}^{-\pi\sqrt{3}}$, as follows from (18). Fig. 5 shows a 3-D view on the flow pattern on the two turns of the Riemann surface. The branch line is the spiral and its continuation (dashed line). The streamlines correspond to the streamlines in Fig. 2. Coming from large y-values, all streamlines follow the convex side of the spiral, turn around the origin and continue along the other spiral side. After crossing the branch line in the left part of Fig. 4, they continue in the right part (in Fig. 5 this branch line is the transition from the upper to the lower turn). The streamline with $\Psi = 0.01$ is difficult to distinguish in the left part; it almost coincides with the convex side of the branch line and spiral, turns around the origin and continues along the concave side. The streamline crosses the branch line while turning around the spiral edge to the convex side of the spiral in the right part. There it turns again around the origin and finally does not follow the spiral contour any more.

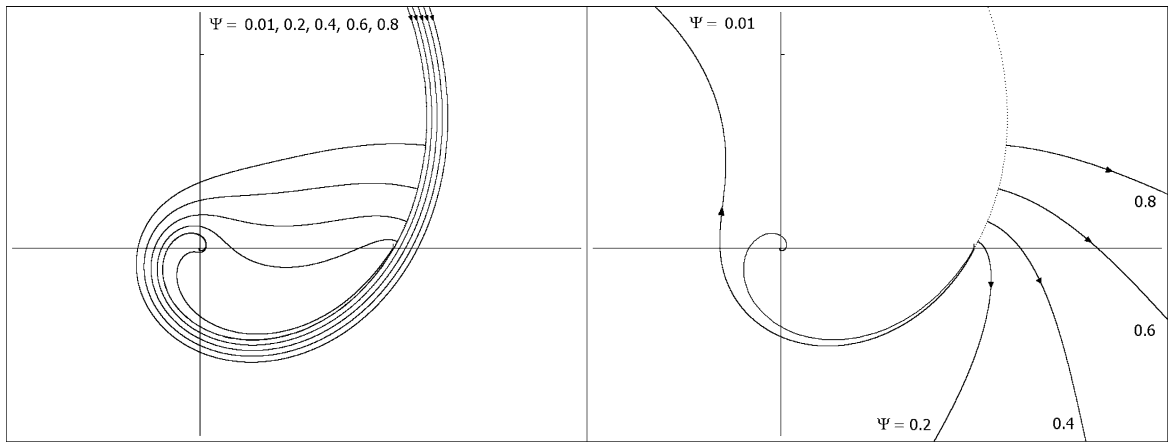

Fig. 4. The flow around the spiral $r = e^{\theta/\sqrt{3}}$ with finite length. The flow is the mapping of the half-plane ($x > 0$) of the flat plate flow in Fig. 2. The left part corresponds to $0 \leqslant \varphi \leqslant \pi/2$, the right part to $-\pi/2 \leqslant \varphi \leqslant 0$.

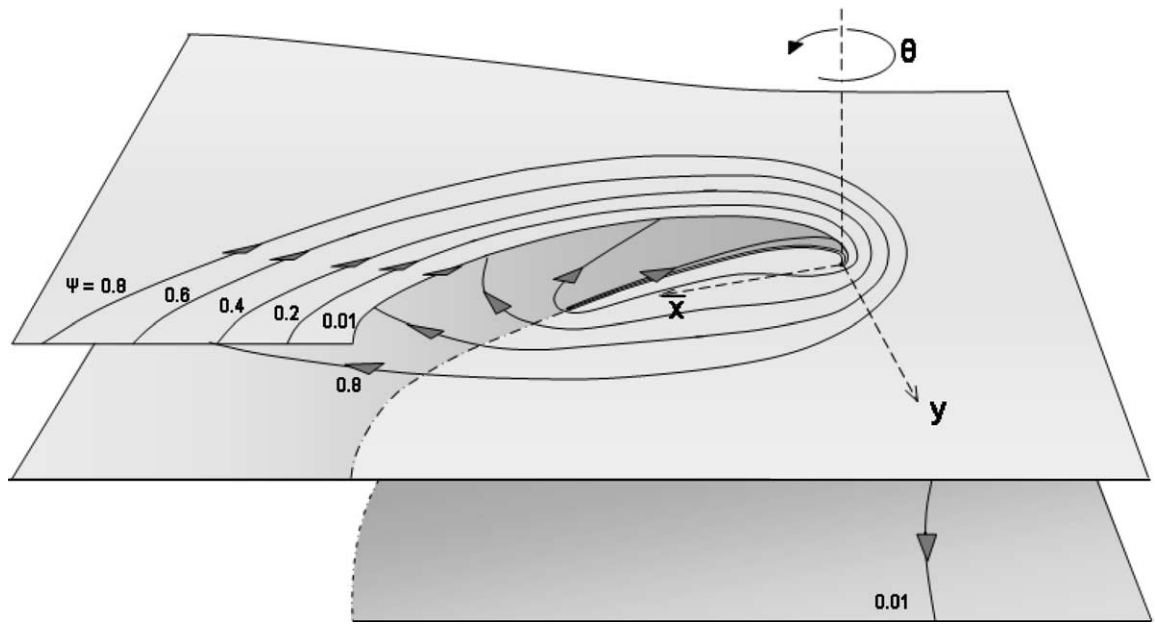

Fig. 5. Three-dimensional representation of the spiral flow on two turns of the Riemann surface, for the finite length spiral $r = e^{\theta/\sqrt{3}}$. The upper turn (light grey) is the left part of Fig. 4, the lower turn (dark grey) the right part.

2.3. The vorticity distribution

The spiral position at which the velocities on both sides of the sheet is determined is denoted as z_{spiral}. These sides are denoted by $+$ and $-$ as shown in (A.2) and Fig. 1. The quantity $(z_{\text{spiral}}/z_{\text{edge}})^{\alpha+i\beta}$ in (26) is evaluated as:

$$\begin{aligned} \left(\frac{z_{\text{spiral}}}{z_{\text{edge}}}\right)_+^{\alpha+i\beta} &= e^{(\theta_{\text{spiral}}-\theta_{\text{edge}})(-(\alpha^2+\beta^2)/\beta)}, \\ \left(\frac{z_{\text{spiral}}}{z_{\text{edge}}}\right)_-^{\alpha+i\beta} &= \left(\frac{z_{\text{spiral}}}{z_{\text{edge}}}\right)_+^{\alpha+i\beta} e^{-2\pi\beta}\cos(2\pi\alpha). \end{aligned} \tag{27}$$

Both expressions are real. Consequently, the velocity at both sides of the sheet is:

$$(v_x + \mathrm{i}v_y)_+ = U_0 \frac{b}{4}\sqrt{\alpha^2+\beta^2}\, \mathrm{e}^{(\alpha/\beta)\theta_{\text{spiral}}}\, \mathrm{e}^{\mathrm{i}(\theta_{\text{spiral}}+\pi/2-\delta)} \frac{\mathrm{e}^{(\theta_{\text{spiral}}-\theta_{\text{edge}})(-(\alpha^2+\beta^2)/\beta)}}{\sqrt{1-\mathrm{e}^{(\theta_{\text{spiral}}-\theta_{\text{edge}})(-(\alpha^2+\beta^2)/\beta)}}}, \tag{28}$$

$$(v_x + \mathrm{i}v_y)_- = U_0 \frac{b}{4}\sqrt{\alpha^2+\beta^2}\, \mathrm{e}^{(\alpha/\beta)\theta_{\text{spiral}}}\, \mathrm{e}^{\mathrm{i}(\theta_{\text{spiral}}+\pi/2-\delta)} \frac{\mathrm{e}^{(\theta_{\text{spiral}}-\theta_{\text{edge}})(-(\alpha^2+\beta^2)/\beta)}\, \mathrm{e}^{-2\pi\beta}\cos(2\pi\alpha)}{\sqrt{1-\mathrm{e}^{(\theta_{\text{spiral}}-\theta_{\text{edge}})(-(\alpha^2+\beta^2)/-\beta)}\, \mathrm{e}^{-2\pi\beta}\cos(2\pi\alpha)}}. \tag{29}$$

From the complex exponential powers in the right-hand side of (28) and (29), it is clear that the velocities are tangential to the sheet when the square root argument in the denominator is positive.

The vortex sheet strength γ equals the difference in velocity at either side of the sheet:

$$\gamma = U_0 \frac{b}{4}\sqrt{\alpha^2+\beta^2}\, \mathrm{e}^{(\theta_{\text{spiral}}-\theta_{\text{edge}})(-(\alpha^2+\beta^2)/\beta)}\, \mathrm{e}^{(\alpha/\beta)\theta_{\text{spiral}}} \left[\frac{\mathrm{e}^{-2\pi\beta}\cos(2\pi\alpha)}{\sqrt{1-\mathrm{e}^{(\theta_{\text{spiral}}-\theta_{\text{edge}})(-(\alpha^2+\beta^2)/\beta)}\, \mathrm{e}^{-2\pi\beta}\cos(2\pi\alpha)}} - \frac{1}{\sqrt{1-\mathrm{e}^{(\theta_{\text{spiral}}-\theta_{\text{edge}})(-(\alpha^2+\beta^2)/\beta)}}} \right]. \tag{30}$$

The total circulation $\Gamma(\theta_{\text{spiral}}) = \int \gamma \,\mathrm{d}\ell$ at the part of the spiral for $\theta \leqslant \theta_{\text{spiral}}$ is, analogous to (21):

$$\Gamma(\theta_{\text{spiral}}) = \sqrt{1+\left(\frac{\alpha}{\beta}\right)^2} \int_{-\infty}^{\theta_{\text{spiral}}} \gamma r_{\text{spiral}}\, \mathrm{d}\theta. \tag{31}$$

Using $A(\theta) = \mathrm{e}^{(\theta-\theta_{\text{edge}})(-(\alpha^2+\beta^2)/\beta)}$ and the substitution of (25), the circulation is given by:

$$\begin{aligned}\Gamma(\theta_{\text{spiral}}) &= -U_0 \frac{b}{4} \int_0^{A(\theta_{\text{spiral}})} \left[\frac{\mathrm{e}^{-2\pi\beta}\cos(2\pi\alpha)}{\sqrt{1-A\,\mathrm{e}^{-2\pi\beta}\cos(2\pi\alpha)}} - \frac{1}{\sqrt{1-A}} \right] \mathrm{d}A \\ &= U_0 \frac{b}{2}\left(\mathrm{e}^{-2\pi\beta}\cos(2\pi\alpha) - 1\right) \mathrm{e}^{(\theta_{\text{spiral}}-\theta_{\text{edge}})(-(\alpha^2+\beta^2)/\beta)}.\end{aligned} \tag{32}$$

For $\theta_{\text{spiral}} = \theta_{\text{edge}}$, the total circulation becomes:

$$\Gamma_{\text{entire spiral}} = U_0 \frac{b}{2}\left(\mathrm{e}^{-2\pi\beta}\cos(2\pi\alpha) - 1\right), \tag{33}$$

which shows that Γ is finite, despite the singular behavior of γ near the edge of the spiral.

2.4. Conditions at infinity

The flow at infinite distance from the spiral is described by (11), when the limit for $|z| \to \infty$ is taken:

$$w(z) \sim \mathrm{i}U_0 z^{(\alpha+\mathrm{i}\beta)/2} \quad \text{for } |z| \to \infty. \tag{34}$$

The velocity is given by:

$$\frac{\partial w(z)}{\partial z} \sim \mathrm{i}U_0 \frac{\alpha+\mathrm{i}\beta}{2} z^{(\alpha+\mathrm{i}\beta-2)/2} \sim U_0 \frac{\alpha^2+\beta^2}{2} r^{(\alpha-2)/2}\, \mathrm{e}^{-(\beta/2)\theta}\, \mathrm{e}^{\mathrm{i}(\delta+((\alpha-2)/2)\theta+(\beta/2)\ln r)} \quad \text{for } |z| \to \infty. \tag{35}$$

The absolute value of the velocity varies with the radius r like $r^{(\alpha-2)/2}$. Since $\alpha \leqslant 3/2$, see Table 1, the velocity always decreases with increasing radius. For increasing θ the velocity increases like $\mathrm{e}^{-(\beta/2)\theta}$ (with β always negative). Therefore, the magnitude of the velocity depends on the turn of the Riemann surface in which the flow is considered.

3. The limit for infinite spiral length

In Section 2.1 it was shown that the limit for infinite spiral length recovers Prandtl's solution, with the constant c determined as U_0/b. The spiral length ℓ is related to b by (21), so for the spiral solutions in Table 1:

$$c = \frac{U_0}{a\ell} \quad \text{with } a = \sqrt{3}, \sqrt{2}, 1 \text{ for } \delta = 30°, 45°, 60°. \tag{36}$$

Expressed in ℓ, the complex potential (11) can be written as a series expansion with respect to ℓ^{-1}, equivalent to (12):

$$w(z) = U_0\left[-\frac{a\ell}{2} + \frac{1}{a\ell}z^{\alpha+\mathrm{i}\beta} - \frac{1}{(a\ell)^3}z^{2(\alpha+\mathrm{i}\beta)}\ldots\right] \tag{37}$$

with a given by (36). The semi-infinite-spiral-flow appears to be the first relevant term in the series expansion of the finite-spiral-flow with respect to ℓ^{-1}.

For the finite length spiral, the circulation up to a certain angle θ_{spiral} is given by (32). With the spiral length ℓ as reference length instead of b and substitution of (19), the circulation becomes for any ℓ:

$$\Gamma(\theta_{\text{spiral}}) = 2\frac{U_0}{a\ell}\left(\mathrm{e}^{-2\pi\beta}\cos(2\pi\alpha) - 1\right)\mathrm{e}^{\theta_{\text{spiral}}(-(\alpha^2+\beta^2)/\beta)} \tag{38}$$

which is the same expression as derived by Prandtl.

For finite values of U_0 the complex potential w and cirulation Γ tend to zero for increasing spiral length ℓ. The explanation for this is the following: the region around the origin of the spiral in Fig. 3, $z \ll z_{\text{edge}}$, is the mapping of the region around the flat plate origin in Fig. 2. For $\rho/(b/2) \to 0$, the flow becomes stagnant, and so does the flow in the z-plane for $|z|/\ell \to 0$. Only when the undisturbed velocity U_0 increases with ℓ, this is avoided. The ratio $c = U_0/(a\ell)$ has fixed values since the dynamic boundary condition determines the admissible values of c (see Table 1). In all cases an infinite value of U_0 is required to avoid the trivial solution of $w \to 0$ for $\ell \to \infty$.

The character of the flow remains unchanged when $\ell \to \infty$: the flow is non-periodic in θ and requires a Riemann surface to be described consistently. The associated flow discontinuity across the branch line, when a 2-D representation is used, still exists but is moved to infinity. For fixed values of c, the circulation at infinity becomes infinite. This confirms the findings of Kambe [7] and Kaneda [8], that the flow solution is ill-posed at infinity.

4. Conclusions

The flow induced by an exponential spiral with a finite length ℓ can be described only on a multi-branched Riemann surface. In a single-branched 2-D plane, the flow is discontinuous across that part of the branch line that is the continuation of the spiral.

The self-similar spiral flows of Prandtl are recovered when the length ℓ of the finite spirals becomes infinite. These flows need to be described on a Riemann surface. The flow discontinuity across the branch line is moved to infinity. When expressed in the 2-D plane, the continuity equation at infinity is not satisfied. This could explain why no physical interpretation of this spiral flow is found so far.

Acknowledgements

The work was partly done during a doctoral thesis study, funded by the Technical University Eindhoven, faculty of Applied Physics, research group Transport Phenomena. Their support, guidance and critical remarks are greatly appreciated.

Appendix A. The boundary conditions for Prandtl's spirals

A.1. The kinematic boundary condition

Prandtl derived that the shape of his spirals with fixed position is given by:

$$\frac{r_{\text{spiral}}}{t^m} = \mathrm{e}^{-(\alpha/\beta)\theta_{\text{spiral}}}. \tag{A.1}$$

With each side of the spiral denoted by $+$ and $-$ as shown in Fig. 1, the polar coordinates are:

$$\begin{aligned} &\frac{r_{\text{spiral}}}{t^m} = \mathrm{e}^{-(\alpha/\beta)\theta_{\text{spiral}}} = \frac{r_+}{t^m} = \frac{r_-}{t^m}, \\ &\theta_+ = \theta_{\text{spiral}}, \\ &\theta_- = \theta_{\text{spiral}} + 2\pi. \end{aligned} \tag{A.2}$$

By substitution of this in (1), the complex potential at the spiral becomes:

$$\left[\Phi_{\text{spiral}}(t,z) + \mathrm{i}\Psi_{\text{spiral}}(t,z)\right]_+ = ct^{2m-1}\left[\frac{r_{\text{spiral}}}{t^m}\,\mathrm{e}^{\mathrm{i}\theta_{\text{spiral}}}\right]^{\alpha+\mathrm{i}\beta} = ct^{2m-1}\,\mathrm{e}^{(-(\alpha^2+\beta^2)/\beta)\theta_{\text{spiral}}}, \tag{A.3}$$

and:

$$\left[\Phi_{\text{spiral}}(t,z)+\mathrm{i}\Psi_{\text{spiral}}(t,z)\right]_{-}=ct^{2m-1}\,\mathrm{e}^{(-(\alpha^2+\beta^2)/\beta)\theta_{\text{spiral}}}\,\mathrm{e}^{-2\pi\beta}\,\mathrm{e}^{\mathrm{i}2\pi\alpha}. \tag{A.4}$$

At the + side, the streamfunction Ψ appears to be zero for any of the constants c, m, α and β. For the sheet to be a stream surface, the value of Ψ at the minus side must have the same value. This is possible only when $\mathrm{e}^{\mathrm{i}2\pi\alpha}$ is real, so when:

$$\sin(2\pi\alpha)=0 \tag{A.5}$$

is satisfied. Apparently the kinematic condition is not distinctive for the determination of the constants c, m and β.

A.2. The dynamic boundary condition for $m=0$

The dynamic boundary condition is analyzed, using the Euler equation in the form:

$$\nabla\left(\frac{\partial\Phi}{\partial t}+p'+\frac{1}{2}|\mathbf{v}|^2\right)=0 \tag{A.6}$$

in which Φ is the real part of (1) with $m=0$, and p' is the pressure divided by the fluid density. Since the flow is irrotational outside the vortex sheet, (A.6) is valid in the entire flow field except at the vortex sheet. Integration across the sheet yields the difference $\Delta=(\,)_{-}-(\,)_{+}$. The sheet is force-free and cannot carry a pressure jump Δp. Therefore the pressure term in the left-hand side vanishes, so integration of (A.6) across the sheet gives:

$$\Delta\left(\frac{\partial\Phi}{\partial t}+\frac{1}{2}|\mathbf{v}|^2\right)=0. \tag{A.7}$$

The unsteady potential Φ equals $\mathrm{Re}(\chi)$, with χ given by (1) with $m=0$, so:

$$\frac{\partial\Phi}{\partial t}=-ct^{-2}\,\mathrm{Re}\left(z^{\alpha+\mathrm{i}\beta}\right)=-ct^{-2}r^{\alpha}\,\mathrm{e}^{-\beta\theta}\cos(\beta\ln r+\alpha\theta). \tag{A.8}$$

The kinematic pressure $\frac{1}{2}|\mathbf{v}|^2$ equals:

$$\frac{1}{2}|\mathbf{v}|^2=\frac{1}{2}c^2t^{-2}\left(\alpha^2+\beta^2\right)r^{2(\alpha-1)}\,\mathrm{e}^{-2\beta\theta}. \tag{A.9}$$

Combining (A.2) with (A.8), (A.9) yields for the dynamic boundary condition:

$$\frac{c}{2}\left(\alpha^2+\beta^2\right)\left(1-\mathrm{e}^{-4\beta\pi}\right)\mathrm{e}^{-((\alpha^2+\beta^2-2\alpha)/\beta)\theta_{\text{spiral}}}=\left(1-\mathrm{e}^{-2\pi\beta}\cos(2\pi\alpha)\right). \tag{A.10}$$

Any set of constants α, β, c that make this equation independent of θ_{spiral} constitutes a valid solution. Independency of θ_{spiral} requires that α and β satisfy the following conditions:

$$\alpha^2+\beta^2-2\alpha=0. \tag{A.11}$$

Together with the condition (A.5), the admissible values of α and β can be calculated. The constant c in (2) is then determined by (A.10).

Appendix B. The edge singularity of the finite spiral

The singular flow around the edge of the spiral (11) induces a suction force F, given by Blasius theorem:

$$F_x-\mathrm{i}F_y=\frac{1}{2}\mathrm{i}\oint_{\text{edge}}\left(\frac{\partial w(t,z)}{\partial z}\right)^2\mathrm{d}z=\frac{U_0^2}{8}\left(\frac{b}{2}\right)^2\left(\alpha^2+\beta^2\right)\oint_{\text{edge}}\left(\mathrm{i}\frac{(z/z_{\text{edge}})^{2(\alpha+\mathrm{i}\beta)}}{1-(z/z_{\text{edge}})^{\alpha+\mathrm{i}\beta}}\frac{\mathrm{e}^{\mathrm{i}(2\delta-\pi)}}{z^2}\right)\mathrm{d}z. \tag{B.1}$$

The transformation $z^*=(z/z_{\text{edge}})^{\alpha+\mathrm{i}\beta}$ yields:

$$F_x-\mathrm{i}F_y=\frac{U_0^2}{8}\left(\frac{b}{2}\right)^2\left(\alpha^2+\beta^2\right)\frac{\mathrm{i}\,\mathrm{e}^{\mathrm{i}(2\delta-\pi)}}{\alpha+\mathrm{i}\beta}\oint_{\text{edge}}\frac{z^*}{1-z^*}\frac{\mathrm{d}z^*}{z} \tag{B.2}$$

which shows that $z^*=1$, or $z=z_{\text{edge}}$, is a single pole in the integrand. The Cauchy integral theorem then gives for the integral $2\pi\mathrm{i}/z_{\text{edge}}$. After substitution of (25) the force on the singularity finally becomes:

$$F_x+\mathrm{i}F_y=-\frac{\pi}{4}U_0^2\sqrt{\alpha^2+\beta^2}\,\frac{(b/2)^2}{r_{\text{edge}}}\,\mathrm{e}^{\mathrm{i}(\theta_{\text{edge}}+\pi/2-\delta)}. \tag{B.3}$$

The force on the singularity appears to be tangent to the spiral at $z = z_{\text{edge}}$, see Fig. 3. The suction force is the equivalent of the suction force at the flat plate edge.

References

[1] H. Kaden, Aufwicklung einer unstabilen Unstetigkeitsfläche, Ing. Archiv. 2 (1931) 140–168.
[2] P.G. Saffman, Vortex Dynamics, in: Cambridge Monographs Mech. Appl. Math., Cambridge University Press, Cambridge, 1992.
[3] L. Prandtl, Über die Entstehung von Wirbeln in der idealen Flüssigkeit, mit Anwendung auf die Tragflügeltheorie und andere Aufgaben, in: von Kármán, Levi-Cevita (Eds.), Vorträge aus dem Gebiete der Hydro- und Aerodynamik, Springer, Berlin, 1922.
[4] R.C. Alexander, Family of similarity flows with vortex sheets, Phys. Fluids 14 (1971) 231.
[5] D. Küchemann, J. Weber, Vortex motions, Z. Angew. Math. Mech. (ZAMM) 45 (1965) 457.
[6] K.W. Mangler, J. Weber, The flow field near the centre of a rolled-up vortex sheet, J. Fluid Mech. 30 (1967) 177.
[7] T. Kambe, Spiral vortex solution of Birkhoff–Rott equation, Physica D 37 (1989) 463.
[8] Y. Kaneda, A family of analytical solutions of the motions of double-branched spiral vortex sheets, Phys. Fluids A 1 (1989) 261.
[9] J.H.B. Smith, Theoretical work on the formation of vortex sheets, in: Küchemann, et al. (Eds.), Prog. Aeron. Sci., vol. 7, Pergamon Press, Oxford, 1966.
[10] H. Lamb, Hydrodynamics, Dover, New York, 1945.